Ninth International Conference on CFD in the Minerals and Process Industries
CSIRO, Melbourne, Australia
10-12 December 2012

IMMERSED BOUNDARY-FINITE DIFFERENCE LATTICE BOLTZMANN METHOD USING TWO RELAXATION TIMES

Roberto Rojas[1], Takeshi Seta[2], Kosuke Hayashi[1], Akio Tomiyama[1*]

[1] Graduate School of engineering, Kobe University, 1-1, Rokkodai, Nada, Kobe, 657-8501, JAPAN

[2] Graduate School of Science and Engineering, Toyama University, 3190, Gofuku, Toyama, 930-8555, JAPAN
*Corresponding author, E-mail address: tomiyama@mech.kobe-u.ac.jp

ABSTRACT

It is known that velocity fields computed by using an immersed boundary-lattice Boltzmann method (IB-LBM) with a single-relaxation time (SRT) show unphysical distortion when the relaxation time, τ, is high. The authors proposed an immersed boundary-finite difference lattice Boltzmann method (IB-FDLBM) using SRT to predict liquid-solid flows. In simulations with IB-FDLBM, numerical errors in the velocity fields appear as in IB-LBMs when τ is high. A two-relaxation time (TRT) collision operator is therefore implemented into IB-FDLBM in this study to reduce numerical errors at high τ. Simulations of circular Couette flows show that the proposed method gives accurate predictions at high τ, provided that the magic parameter, which is a function of the relaxation times, is less than unity. In addition, predicted drag coefficients of a circular cylinder and a sphere at low Reynolds numbers show reasonable agreements with theoretical solutions and measured data.

NOMENCLATURE

A	negative viscosity term
c	lattice speed, $c = 1$
$\boldsymbol{c}$	discrete particle velocity, $\boldsymbol{c} = (c_x, c_y)$
C_D	drag coefficient
D	particle diameter
f	particle velocity distribution function
f^{eq}	equilibrium distribution function
f^{+}	symmetric part of distribution function
f^{-}	anti-symmetric part of distribution function
$f^{eq,+}$	symmetric part of equilibrium distribution function
$f^{eq,-}$	anti-symmetric part of equilibrium distribution function
$\boldsymbol{F}$	external force, $\boldsymbol{F} = (F_x, F_y)$
F_D	drag force
G_i	direct forcing term for f_i
l	norm
N_m	number of Lagrangian points at immersed boundary
p	pressure
Q	number of discrete particle velocities
Re	Reynolds number
R_{in}	radius of inner cylinder
R_{out}	radius of outer cylinder
t	time
$\boldsymbol{u}$	fluid velocity, $\boldsymbol{u} = (u, v)$
u_θ	azimuthal velocity component
$\boldsymbol{u}_P$	velocity of solid body
u_T	analytical azimuthal velocity component
U_0	free stream velocity
U_θ	rotation velocity of circular cylinder
W	weighting function
$\boldsymbol{x}$	Eulerian coordinates, $\boldsymbol{x} = (x, y)$
$\boldsymbol{X}_L$	coordinates of Lagrangian point, $\boldsymbol{X}_L = (X_L, Y_L)$
Δ	domain of the smoothed delta function
δ	smoothed-delta function
δ_h	one-dimensional smoothed-delta function
ΔS	area segment of solid body
Δt	time step size
ΔV	computational cell volume
Δx	lattice width in the x direction
Δy	lattice width in the y direction
Δz	lattice width in the z direction
γ	Euler constant
ε	Knudsen number
Λ	magic parameter
μ	viscosity
ν	kinematic viscosity
ρ	density
τ_+	relaxation time for f^+ in two-time relaxation model
τ_-	relaxation time for f^- in two-time relaxation model
Ω	collision operator
Subscript	
i	direction of discrete particle velocity
$\bar{i}$	direction opposite to i
I,J,K	indexes of lattice point
L	index of Lagrangian node
Superscript	
n	discrete time

INTRODUCTION

The lattice Boltzmann method is now regarded as one of the promising methods for simulating fluid flows. Due to its simplicity and suitability for parallel computation, it has been widely used for predicting various flows such as turbulent flows (Martinez et al., 1994) and two-phase flows (Shan and Chen, 1993). In particular, the combination of the immersed boundary method and lattice Boltzmann method (IB-LBM) using a single relaxation time (SRT) has been adopted to reasonably predict liquid-solid two-phase flows (Feng and Michaelides, 2004; Feng and Michaelides, 2005; Feng and Michaelides, 2009; Dupuis et al., 2008). However, Le & Zhang (2009) carried out simulations of circular Couette flows and pointed out that large non-physical velocity distortion in the vicinity of immersed boundaries is caused when the relaxation time, τ, is high.

The authors recently proposed a combination of a finite difference lattice Boltzmann method using the single relaxation time and the immersed boundary method (IB-FDLBM), which can stably and efficiently simulate liquid-solid flows (Rojas et al., 2011). In IB-FDLBM, an additional collision term (Tsutahara et al., 2002), which works as a negative viscosity in the macroscopic level, is used to improve the numerical stability, and allows us to simulate flows at high Reynolds numbers. However the velocity distortion near the immersed boundary appears as in IB-LBM when τ is high.

A two-relaxation time (TRT) collision model (Ginzburg et al., 2008) is, therefore, implemented into the IB-FDLBM in this study to reduce the numerical error at high relaxation times. One relaxation time of TRT is used to define the viscosity of the flow, and the other relaxation time is used to improve the accuracy. Simulations of circular Couette flows are carried out for a wide range of relaxation times to validate the present method. Predicted velocity distributions and velocity profiles are compared with the predictions obtained by IB-FDLBM with SRT and an analytical solution. Flow past a circular cylinder at a low Reynolds number is also simulated and the drag coefficients obtained by using SRT and TRT collision models are compared with a theoretical solution. Simulations of flows past a sphere at low and high Reynolds numbers are also carried out. In appendix A, the Chapman-Enskog expansion is applied to IB-FDLBM with TRT to show the recovery of the macroscopic conservation equations for incompressible Newtonian flows, i.e., the continuity and Navier-Stokes equations.

NUMERICAL METHOD

The discrete Boltzmann equation with the direct forcing term, G_i, is given by

$$\frac{\partial f_i}{\partial t} + \boldsymbol{c}_i \cdot \nabla[\, f_i + A\Omega_i \,] = \Omega_i + G_i \tag{1}$$

where f_i is the distribution function for the ith component of discrete velocity and A is a parameter, which works as a negative viscosity in the macroscopic level (Tsutahara et al., 2002). The collision operator Ω_i using two relaxation times is given by (Ginzburg et al., 2008):

$$\Omega_i = -\frac{1}{\tau_+}[\, f_i^{+} - f_i^{eq,+}] - \frac{1}{\tau_-}[\, f_i^{-} - f_i^{eq,-}] \tag{2}$$

where τ_+ and τ_- are the relaxation times for the symmetric part, f^+, of the distribution function and for the anti-symmetric one, f^-, respectively. The former is used for determining the kinematic viscosity, and the latter is used to improve numerical stability and accuracy. The distribution functions, f^+, f^-, $f^{eq,+}$ and $f^{eq,-}$,are defined by

$$f_i = f_i^{+} + f_i^{-} \tag{3}$$

$$f_i^{+} = \frac{f_i + f_{\bar{i}}}{2} \tag{4}$$

$$f_i^{-} = \frac{f_i - f_{\bar{i}}}{2} \tag{5}$$

$$f_i^{eq} = f_i^{eq,+} + f_i^{eq,-} \tag{6}$$

$$f_i^{eq,+} = \frac{f_i^{eq} + f_{\bar{i}}^{eq}}{2} \tag{7}$$

$$f_i^{eq,-} = \frac{f_i^{eq} - f_{\bar{i}}^{eq}}{2} \tag{8}$$

where f_i^{eq} is the equilibrium distribution function and the subscript $\bar{i}$ denotes the direction opposite to i. The macroscopic fluid density, ρ, velocity, $\boldsymbol{u}$, and f_i^{eq} in the D2Q9 and D3Q19 models are given by

$$\rho = \sum_{i=0}^{Q-1} f_i \tag{9}$$

$$\rho \boldsymbol{u} = \sum_{i=0}^{Q-1} \boldsymbol{c}_i f_i \tag{10}$$

$$f_i^{eq} = W_i \rho \left[1 + \frac{3(\boldsymbol{c}_i \cdot \boldsymbol{u})}{c^2} + \frac{9(\boldsymbol{c}_i \cdot \boldsymbol{u})^2}{2c^4} - \frac{3\boldsymbol{u} \cdot \boldsymbol{u}}{2c^2} \right] \tag{11}$$

where W_i is the weighting function and c the lattice velocity. In the D2Q9 model, W_0 = 4/9, W_i = 1/9 for i = 1-4 and W_i = 1/36 for i = 5-8. In the D3Q19 model, W_0 = 1/3, W_i = 1/18 for i = 1-6 and W_i = 1/36 for i = 7-18. The kinematic viscosity is given by

$$\nu = \frac{c^2}{3}(\tau_+ - A) \tag{12}$$

The relaxation parameter, τ_-, is determined through the magic parameter,

$$\Lambda = (\tau_+ - A)(\tau_- - A) \tag{13}$$

The value of Λ should be tuned to improve the numerical stability and accuracy. In some cases, the optimum value of Λ can be obtained theoretically (Ginzburg et al., 2008; Seta et al., 2012).

Fluid motion is computed at Eulerian grid points, $\boldsymbol{x}_{IJK}$ = (x_I, y_J, z_K), by solving Eq. (1), whereas solid boundaries immersed in the flow field are represented using Lagrangian points, $\boldsymbol{X}_L$ = (X_L, Y_L, Z_L). The external force, $\boldsymbol{F}(\boldsymbol{X}_L,t)$, acting on the fluid to impose the no-slip boundary condition is given by (Dupuis et al., 2008)

$$\boldsymbol{F}(\boldsymbol{X}_L,t) = \rho \frac{\boldsymbol{u}_P(\boldsymbol{X}_L,t) - \boldsymbol{u}(\boldsymbol{X}_L,t)}{\Delta t} \tag{14}$$

where Δt is the time step, $\boldsymbol{u}_P(\boldsymbol{X}_L, t)$ the velocity at the Lth Lagrangian point, and $\boldsymbol{u}(\boldsymbol{X}_L, t)$ the velocity interpolated by using

$$\boldsymbol{u}(\boldsymbol{X}_L,t) = \sum_{\boldsymbol{x}_{IJK} \in \Delta} \boldsymbol{u}(\boldsymbol{x}_{IJK},t)\delta(\boldsymbol{x}_{IJK} - \boldsymbol{X}_L)\Delta V \tag{15}$$

where δ is the smoothed-delta function (Le and Zhang, 2009), ΔV the volume of a computational cell, and Δ the domain in which $\delta \neq 0$. The delta function is given by

$$\delta(\boldsymbol{x}_{IJK}-\boldsymbol{X}_L)=\delta_h\left(\frac{x_I-X_L}{\Delta x}\right)\delta_h\left(\frac{y_J-Y_L}{\Delta y}\right)\delta_h\left(\frac{z_K-Z_L}{\Delta z}\right) \quad (16)$$

where Δx, Δy and Δz are the lattice spacings in the x, y and z directions, respectively, and δ_h is the one-dimensional smoothed-delta function, for which the following 4-point cosine delta function is adopted:

$$\delta_h(r)=\begin{cases}\frac{1}{4}\left[1+\cos\left(\frac{\pi|r|}{2}\right)\right] & \text{for } |r|\le 2\\ 0 & \text{for } |r|>2\end{cases} \quad (17)$$

Then the force calculated using Eq. (14) is distributed onto the Eulerian grid points by using the delta function:

$$\boldsymbol{F}(\boldsymbol{x}_{IJK},t)=\sum_{L=1}^{N_m}\boldsymbol{F}(\boldsymbol{X}_L,t)\delta(\boldsymbol{x}_{IJK}-\boldsymbol{X}_L)\Delta S\,\Delta x \quad (18)$$

where N_m is the number of Lagrangian points and ΔS the area segment of a solid body. The direct forcing term is given by

$$G_i(\boldsymbol{x}_{IJK},t)=3W_i\boldsymbol{c}_i\cdot\boldsymbol{F}(\boldsymbol{x}_{IJK},t) \quad (19)$$

A second-order Runge-Kutta method is used for the time integration of Eq. (1):

$$f_i^{n+1/2}=f_i^n+\frac{\Delta t}{2}[-\boldsymbol{c}_i\cdot\nabla(f_i+A\Omega_i)+\Omega_i+G_i]^n \quad (20)$$

$$f_i^{n+1}=f_i^n+\Delta t[-\boldsymbol{c}_i\cdot\nabla(f_i+A\Omega_i)+\Omega_i+G_i]^{n+1/2} \quad (21)$$

where the superscript n is the discrete time, i.e. $t = n\Delta t$. The advection term is discretized using a third-order upwind scheme.

SIMULATION OF CIRCULAR COUETTE FLOWS

Simulations of two-dimensional circular Couette flows are carried out to demonstrate that the proposed method can remove unphysical distortions in a velocity field at high relaxation times. Figure 1 shows the computational setup. The numbers of lattice points in the x and y directions are 201 and 201. The outer cylinder is at rest, while the inner cylinder is rotating at the azimuthal velocity U_θ = 0.01. The radii, R_{out} and R_{in}, of the outer and inner cylinders are 70 and 45, respectively. The number of Lagrangian points is 440 for each cylinder surface. The number of these points is determined so as to make the spacing between two points on the outer cylinder comparable to the grid spacing. Higher spatial resolutions, e.g. 880 and 220, were also tested and no significant differences were found in the results. Periodic boundary conditions are adopted for all the domain boundaries.

First, IB-FDLBM with SRT is used to simulate the flows. The negative viscosity term, A, is kept at 0.5. Figure 2 shows the azimuthal velocity component, u_θ. The numerical error in velocity increases with τ and the non-symmetric velocity fields appear at $\tau \gtrsim 10$. The distortion in velocity field at high τ is clearer in Fig. 3. The circular Couette flows are then simulated using TRT. The negative viscosity term is kept at 0.5, and the magic parameter Λ is set at 1/4. As shown in Fig. 4, the velocity field is not distorted even at high τ_+. A comparison between velocity profiles along a horizontal cross-section obtained with SRT and TRT is shown in Fig. 5. The solid line in the fluid region is the analytical solution given by

$$\frac{u_T}{U_\theta}=\left(\frac{R}{R_{out}}-\frac{R_{out}}{R}\right)\Big/\left(\frac{R_{in}}{R_{out}}-\frac{R_{out}}{R_{in}}\right) \quad (22)$$

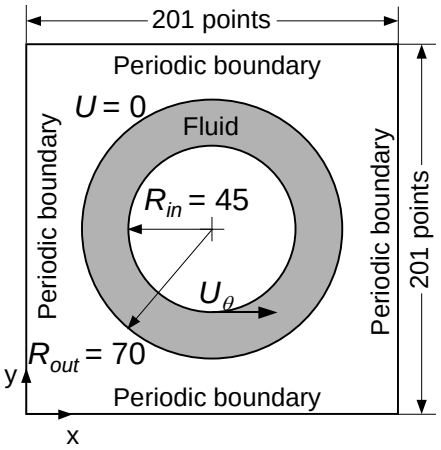

Figure 1: Computational domain for circular Couette flows.

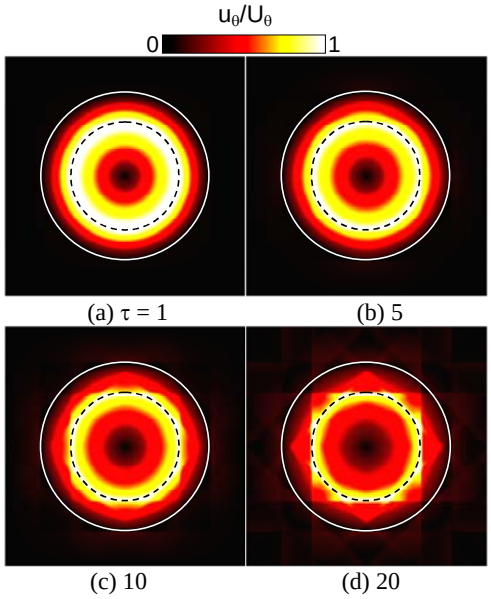

Figure 2: Velocity distributions predicted by using IB-FDLBM with SRT (A = 0.5).

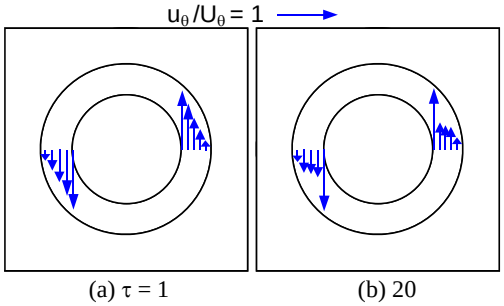

Figure 3: Velocity vector along the x-axis predicted by using IB-FDLBM with SRT (A = 0.5).

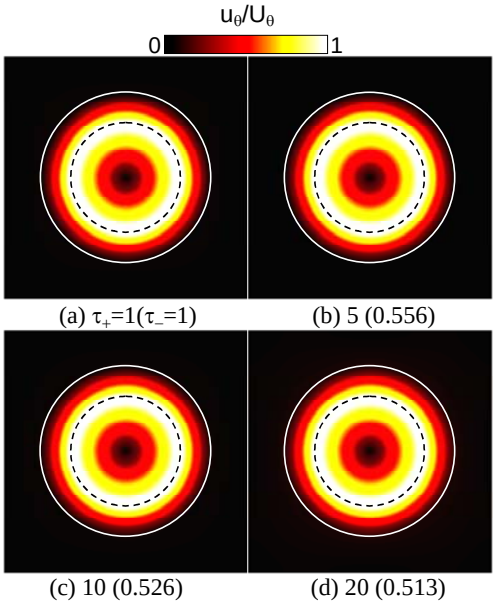

Figure 4: Velocity distributions predicted by using IB-FDLBM with TRT (A = 0.5 and Λ = 1/4).

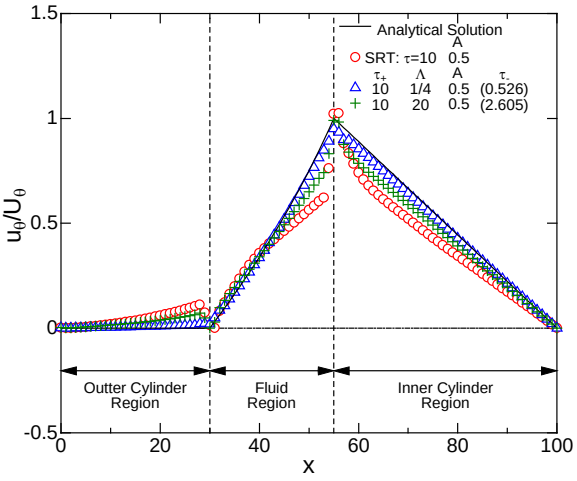

Figure 5: Velocity profile of circular Couette flows along a horizontal line (τ =10).

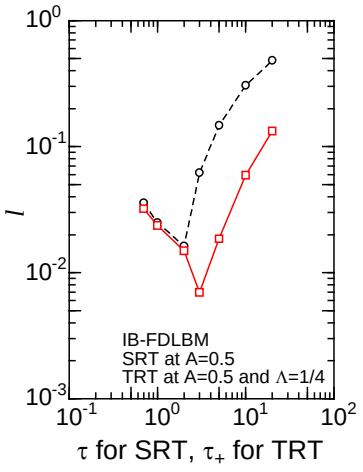

Figure 6: Norms obtained by using SRT and TRT at different relaxation times.

The solution obtained with TRT and Λ = 1/4 agrees well with the analytical solution, whereas that obtained with SRT largely differs from the analytical solution, especially in the vicinity of the immersed boundary. Various values of Λ are tested to confirm that accurate predictions are obtained only when the magic parameter is less than about one. For instance, the solution obtained with Λ = 20 differs from the analytical solution as shown in Fig. 5. Figure 6 shows the errors in velocity distribution predicted using SRT and TRT collision terms, where l is the norm defined by

$$l = \max_{IJ \in fluid} \left| \frac{u_\theta - u_T}{u_T} \right| \qquad (23)$$

In both cases, the error decreases with increasing τ up to around τ = 2 and then increases at higher τ. The reason of this tendency is as follows. The direct forcing method enforces $\boldsymbol{u}_P(\boldsymbol{X}_L) = \boldsymbol{u}(\boldsymbol{X}_L)$ but does not ensure $\boldsymbol{u}_{theory}(\boldsymbol{X}_L) = \boldsymbol{u}(\boldsymbol{X}_L)$ due to the diffusive nature of δ_h. Because of this, the predicted fluid velocity in the vicinity of the rotating cylinder is slightly higher than the theoretical one at low τ. Then, the predicted velocity decreases as τ increases and approaches the theoretical velocity at τ = 2 in SRT and τ_+ = 3 in TRT, where the norms take the minimum value. Then, the norms increase with τ at high τ since the velocity continues to decrease with increasing τ. The errors are smaller in TRT than in SRT.

FLOW PAST A CIRCULAR CYLINDER AT A LOW REYNOLS NUMBER

A flow past a circular cylinder at a low Reynolds number, Re = 0.1, is simulated to examine the accuracy of the proposed method at a high relaxation time. The computational domain is shown in Fig. 7. The dimensions of the domain are 50D and 40D in the x and y directions. The cylinder is located at (20D, 20D) and the ratio, $D/\Delta x$, is 40. The number of Lagrangian points, which are evenly distributed at the cylinder surface, is 126. A is set at 0.5 for both models, and therefore, τ in SRT and τ_+ in TRT are 60.5. The magic parameter of TRT is 1/4. The uniform flow along the x-axis enters from the left boundary. The right boundary is continuous outflow. The top and bottom boundaries are slip wall. The drag force, F_D, is calculated by summing up $\boldsymbol{F}(\boldsymbol{X}_L,t)$ for all the Lagrangian points:

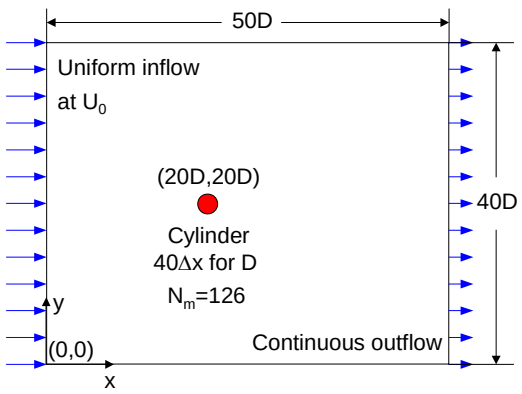

Figure 7: Computational domain for flows past a circular cylinder.

$$F_D = -\sum_{L=1}^{N_m} F_x(\boldsymbol{X}_L, t)\Delta S\,\Delta x \qquad (24)$$

where $F_x(\boldsymbol{X}_L,t)$ is the x component of $\boldsymbol{F}(\boldsymbol{X}_L,t)$. The drag coefficient, C_D, is defined by

$$C_D = \frac{F_D}{\frac{1}{2}\rho U_0^2 D} \qquad (25)$$

The predicted drag coefficients are compared with the following theoretical solution (Lamb, 1911):

$$C_D = \frac{8\pi}{Re\left(\frac{1}{2} - \gamma - \ln\frac{Re}{8}\right)} \qquad (26)$$

where $\gamma = 0.57721$ is the Euler constant. Table 1 shows a comparison of the drag coefficients. The error in the drag coefficient is very large in SRT, whereas it is much lower in TRT.

FLOW PAST A SPHERE

Simulations of flows past a sphere at low and high Reynolds numbers are carried out. The dimensions of the domain are 50D, 40D and 40D in the x, y and z directions, respectively. The sphere is located at (20D, 20D, 20D) and the ratio, $D/\Delta x$, is 40. Lagrangian points are generated using a method proposed by Feng & Michaelides (2005). The number of Lagrangian points at the sphere surface is 4958 and A is set at 0.5. The magic parameter of TRT is 1/4. The boundary conditions are similar to those used for the two-dimensional circular cylinder.

Table 1: Comparison of drag coefficients of a circular cylinder at Re = 0.1.

	Re = 0.1	Error [%]
Theoretical Solution (Lamb, 1911)	58.4	-
SRT model (present)	40.3	31.0
TRT model (present)	61.3	5.0

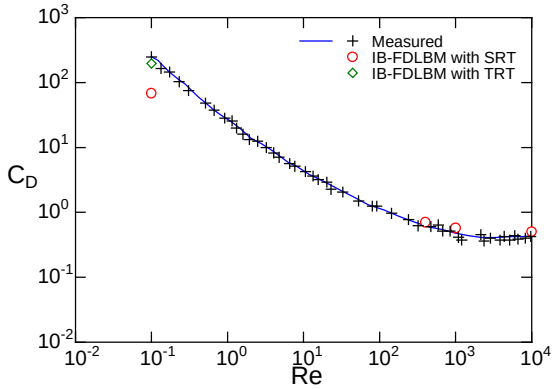

Figure 8: Drag coefficients of sphere.

The drag coefficients are plotted against the Reynolds number in Fig. 8. Good agreements between measured data (Wieselsberger, 1922) and the predictions at high Reynolds numbers, i.e. Re = 400, 1000 and 10000, are obtained using SRT. The relaxation time τ ranges from 0.515 to 0.5006 at these Reynolds numbers. The C_D at Re = 0.1, however, differs from the measured value due to the high relaxation time; τ = 60.5. On the other hand, TRT gives a better prediction at the low Reynolds number than SRT.

CONCLUSION

A two-relaxation collision model was implemented into the immersed boundary-finite difference lattice Boltzmann method to reduce numerical errors appearing at high relaxation times. Simulations of circular Couette flows and flows past a circular cylinder and a sphere were carried out to examine the applicability of the method to low Re flows. As a result, the following conclusions are obtained: (1) TRT reduces non-physical distortion of the fluid velocity in the vicinity of immersed boundaries of flows at high relaxation times, (2) accurate predictions are obtained only when the magic parameter is less than about one, and (3) flows past a circular cylinder and a sphere at low Reynolds numbers are reasonably predicted with TRT.

ACKNOWLEDGEMENTS

This work has been supported by the Japan Society for the Promotion of Science (JSPS) (grants-in-aid for scientific research (B) No. 24360070).

REFERENCES

DUPUIS, A., CHATELAIN, P., KOUMOUTSAKOS, P., (2008), "An immersed boundary-lattice Boltzmann method for the simulation of the flow past an impulsively started cylinder", *J. of Computational Physics*, 227, 4486-4498.

FENG, Z.-G. and MICHAELIDES, E.E., (2004), "The immersed boundary-lattice Boltzmann method for solving fluid-particles interaction problems", *J. of Computational Physics*, 195, 602-628.

FENG, Z.-G. and MICHAELIDES, E.E., (2005), "Proteus: a direct forcing method in the simulations of particulate flows", *J. of Computational Physics*, 202, 20-51.

FENG, Z.-G. and MICHAELIDES, E.E., (2009), "Robust treatment of no-slip boundary condition and velocity updating for the lattice-Boltzmann simulation of particulate flows", *Computers and Fluids*, 38, 370-381.

GINZBURG, I., VERHAEGHE, F., d'HUMIERES, D., (2008), "Two-relaxation-time lattice Boltmann scheme: about parametrization, velocity, pressure and mixed boundary conditions", *Communication in Computational Physics*, **3(2),** 427-478.

LAMB, H., (1911), "On the uniform motion of a sphere through a viscous fluid", *Phil. Mag.*, 6(xxi), 112.

LE, G. and ZHANG T., (2009), "Boundary slip from the immersed boundary lattice Boltzmann models", *Physical Review E*, **79,** 026701.

MARTINEZ, D. O.,MATTHAEUS, W. H., CHEN, S., MONTGOMERY, D. C., (1994), "Comparison of spectral method and lattice Boltzmann simulations of two-dimensional hydrodynamics", *Physics of Fluids*, 6, 1285-1298.

ROJAS, R., SETA, T., HAYASHI, K., TOMIYAMA A., (2011), "Immersed boundary-finite difference lattice Boltzmann method for liquid-solid two-phase flows", *J. of Fluid Science and Technology*, 6(6), 1051-1064.

SETA, T., ROJAS, R., HAYASHI, K., TOMIYAMA, A., (2012), "Reduction of boundary slip from the immersed boundary-lattice Boltzmann method by two-relaxation-time", *JSMF Annual Meeting 2012*, B233, 168-169. (in Japanese)

SHAN, X. and CHEN, H., (1993), "Lattice Boltzmann model for simulating flows with multiple phases and components", *Physical Review E*, 47(3), 1815-1820.

TSUTAHARA, M., KURITA, M., IWAGAMI, T., (2002), "A study of new finite difference lattice Boltzmann model", *Transaction of Japanese Society of Mechanical Engineers*, Series B, 68(665).

WIESELSBERGER, C., (1922), "Further information on the laws of fluid resistance", *National Advisory Committee for Aeronautics*, 121.

APPENDIX A

Derivation of Macroscopic Equations

The macroscopic equations, i.e. the continuity and the Navier -Stokes equations, are obtained by the Chapman-Enskog expansion:

$$f_i = f_i^{(0)} + \varepsilon f_i^{(1)} + \varepsilon^2 f_i^{(2)} + ... \quad (A1)$$

$$f_i^{\pm} = f_i^{\pm(0)} + \varepsilon f_i^{\pm(1)} + \varepsilon^2 f_i^{\pm(2)} + ... \quad (A2)$$

$$\frac{\partial}{\partial t} = \varepsilon \frac{\partial}{\partial t_1} + \varepsilon^2 \frac{\partial}{\partial t_2} \quad (A3)$$

$$\frac{\partial}{\partial x_\alpha} = \varepsilon \frac{\partial}{\partial x_\alpha} \quad (A4)$$

where ε is the Knudsen number. The first four moments of the equilibrium distribution function are

$$\sum f_i^{eq} = \sum f_i^{eq,+} = \rho \quad (A5)$$

$$\sum f_i^{eq} c_{i\alpha} = \sum f_i^{eq,-} c_{i\alpha} = \rho u_\alpha \quad (A6)$$

$$\sum f_i^{eq} c_{i\alpha} c_{i\beta} = \sum f_i^{eq,+} c_{i\alpha} c_{i\beta} = \frac{1}{3}\rho\delta_{\alpha\beta} + \rho u_\alpha u_\beta \quad (A7)$$

$$\sum f_i^{eq} c_{i\alpha} c_{i\beta} c_{i\gamma} = \sum f_i^{eq,-} c_{i\alpha} c_{i\beta} c_{i\gamma} = \rho u_\alpha u_\beta u_\gamma + \frac{1}{3}\rho\left(u_\alpha\delta_{\beta\gamma} + u_\beta\delta_{\alpha\gamma} + u_\gamma\delta_{\alpha\beta}\right) \quad (A8)$$

The distribution functions $f_i^{(m)}$ and $f_i^{\pm(m)}$ satisfy

$$\sum f_i^{(m)} = 0 \quad (A9)$$

$$\sum f_i^{(m)} c_{i\alpha} = 0 \quad (A10)$$

$$\sum f_i^{(m)\pm} = 0 \quad (A11)$$

$$\sum f_i^{(m)\pm} c_{i\alpha} = 0 \quad (A12)$$

for $m \geq 1$. Substituting Eqs. (A1)-(A4) into Eq. (1) yields the following equations for the orders of ε^0, ε^1 and ε^2:

$$\varepsilon^0 : \quad f_i^{(0)} = f_i^{eq} \quad (A13)$$

$$\varepsilon^1 : \frac{\partial}{\partial t_1} f_i^{(0)} + c_{i\alpha}\frac{\partial}{\partial x_\alpha} f_i^{(0)} = -\frac{1}{\tau_+} f_i^{(1)+} - \frac{1}{\tau_-} f_i^{(1)-} \quad (A14)$$

$$\varepsilon^2 : \frac{\partial}{\partial t_1} f_i^{(1)} + \frac{\partial}{\partial t_2} f_i^{(0)} + c_{i\alpha}\frac{\partial}{\partial x_\alpha} f_i^{(1)} - Ac_{i\alpha}\frac{\partial}{\partial x_\alpha}\left[\frac{1}{\tau_+} f_i^{(1)+} + \frac{1}{\tau_-} f_i^{(1)-}\right] = -\frac{1}{\tau_+} f_i^{(2)+} - \frac{1}{\tau_-} f_i^{(2)-} \quad (A15)$$

To obtain $f_i^{(1)}$, the symmetric and anti-symmetric parts are derived from Eq. (A14)

$$f_i^{(1)} = -\tau_+\left(\frac{\partial}{\partial t_1} f_i^{(0)+} + c_{i\alpha}\frac{\partial}{\partial x_\alpha} f_i^{(0)-}\right) - \tau_-\left(\frac{\partial}{\partial t_1} f_i^{(0)-} + c_{i\alpha}\frac{\partial}{\partial x_\alpha} f_i^{(0)+}\right) \quad (A16)$$

Summing Eqs. (A14) and (A15) over *i* yields

$$\frac{\partial}{\partial t_1}\rho + \frac{\partial}{\partial x_\alpha}\rho u_\alpha = 0 \quad (A17)$$

$$\frac{\partial}{\partial t_2}\rho = 0 \quad (A18)$$

Combining Eq. (A17) and (A18) gives the continuity equation:

$$\frac{\partial}{\partial t}\rho + \frac{\partial}{\partial x_\alpha}\rho u_\alpha = 0 \quad (A19)$$

Multiplying Eqs. (A14) and (A15) by $c_{i\alpha}$ and summing the resultant equations over *i* yields

$$\frac{\partial \rho u_\alpha}{\partial t_1} + \frac{\partial}{\partial x_\beta}\left(\frac{1}{3}\rho\delta_{\alpha\beta} + \rho u_\alpha u_\beta\right) = 0 \quad (A20)$$

$$\frac{\partial \rho u_\alpha}{\partial t_2} - \left(\tau_+ - A\right)\frac{\partial}{\partial x_\beta}\left(\frac{1}{3}\rho\frac{\partial u_\alpha}{\partial x_\beta} + \frac{1}{3}\rho\frac{\partial u_\beta}{\partial x_\alpha}\right) + \left(\tau_+ - A\right)\frac{\partial}{\partial x_\alpha}\left(\frac{\partial u_\alpha u_\beta u_\gamma \rho}{\partial x_\beta}\right) = 0 \quad (A21)$$

Combining Eqs. (A20) and (A21) yields the incompressible Navier-Stokes equation:

$$\frac{\partial \rho u_\alpha}{\partial t} + \frac{\partial \rho u_\alpha u_\beta}{\partial x_\beta} = -\frac{\partial p}{\partial x_\alpha} + \frac{\partial}{\partial x_\beta}\left[\mu\left(\frac{\partial u_\alpha}{\partial x_\beta} + \frac{\partial u_\beta}{\partial x_\alpha}\right)\right] \quad (A22)$$

where the pressure p and the viscosity μ are given by $p=\rho/3$ and $\mu = \rho\nu$, respectively.